Supplementary Information (SI) for Chemical Science.

Single-B/N MR-TADF Emitters Enhancing Electroluminescence Efficiency via "Terminal Engineering" Strategy

Hengxuan Qi[ab+], Hao Liu[c+], Deli Li[d+], Lin Wu[b]*, Jiasen Zhang[b], Huaxin Li[b], Ziru Xin[b], Chao Xia[b], Ruixiang Peng[b]*, Wenjun Wang[a], Zujin Zhao[c]*, Wei Li[b]*, and Ziyi Ge[b]*

a. *School of Physical Science and Information Technology, Liaocheng University, Liaocheng 2520259, P. R. China.*

b. *Zhejiang Provincial Engineering Research Center of Energy Optoelectronic Materials and Devices, Ningbo Institute of Materials Technology and Engineering, Chinese Academy of Sciences, Ningbo, 315201, P. R. China*
Center of Materials Science and Optoelectronics Engineering, University of Chinese Academy of Sciences, P. R. China

c. State Key Laboratory of Luminescent Materials and Devices and Institute of South China University of Technology, Wushan Road 381, Tianhe District, Guangzhou 510640, Guangdong Province, P. R. China.

d. Institute for Smart Materials & Engineering, University of Jinan, No. 336 Nanxinzhuang West Road, Jinan, 250022, P. R. China

+.These authors contributed equally to this work.

*Corresponding author

E-mail: pengrx@nimte.ac.cn; liwei1987@nimte.ac.cn; geziyi@nimte.ac.cn; mszjzhao@scut.edu.cn.

1. General Information

The ^{1}H NMR spectra were recorded on Bruker NMR spectrometers operating at 400 and 151 MHz. Mass spectra were recorded by an AB Sciex TripleTOF 4600 mass analyzer (AB Sciex, Framingham, MA, USA). UV-vis spectra were recorded using Perkin-Elmer Lambda 950-PKA UV-Vis. All low-temperature steady-state fluorescence and phosphorescence spectra were recorded using a Horiba Jobin Yvon FluoroMax-4 Spectrofluorometer equipped with a Dewar flask. Low-temperature fluorescence spectra can be measured using the stable-state fluorescence mode without time delay. Low-temperature phosphorescence spectra can be recorded using phosphorescence mode after a time delay of 0.05-50 ms (adjustable delay time range: 50 μs–100 ms) to eliminate the influence of low-temperature fluorescence spectra. Cyclic voltammetry measurements were conducted using the electrochemical workstation Multiautolab M204. Photoluminescence quantum yields (PLQYs) in doped films were measured utilizing an integrating sphere of a Hamamatsu absolute PLQY spectrometer (C11347-01). Thermogravimetric analyses (TGA) were conducted on a Netzsch TGA 2019F1, and differential scanning calorimetry (DSC) measurements were carried out on a Netzsch DSC 214. Both TGA and DSC measurements were under N_2 flow.

1.1. Quantum Chemical Method

All simulations were performed using the Gaussian 16 program package [1]. The ground-state (S_0) geometries were optimized for all the investigated molecules using the B3LYP/6-31g(d, p) method in vacuum, with the initial guess set to the vacuum-optimized geometries. The excited state was optimized using TD-DFT/B3LYP/6-31g(d,p) in toluene with the polarizable continuum model (PCM).[2] Frontier molecular orbitals (FMOs), natural transition orbitals (NTOs), and root-mean-square displacements (RMSDs) were further analyzed using the wavefunction analyzers Multiwfn and VMD, with results obtained from Gaussian 16.[3] The Huang-Rhys (HR) factors were determined with the DUSHIN module in MOMAP (Molecular Materials Property Prediction Package), and the calculated spectra were obtained using Frank-Condon (FC) analysis with a sum-over-states approach implemented in the MOMAP software.[4]

1.2. Device Fabrication and Characterization

Glass substrates pre-coated with a 95-nm-thick layer of indium tin oxide (ITO) with a sheet resistance of 10 Ω per square were thoroughly cleaned in an ultrasonic bath containing tetrahydrofuran, isopropyl alcohol, detergent, and deionized water. They were then treated with O_2 plasma for 5 minutes in sequence. Organic layers were deposited onto ITO-coated glass substrates by thermal evaporation under high-vacuum conditions (~10^{-5} Pa). The cathode was patterned using a shadow mask with 3 mm x 3 mm openings. Deposition rates are

1 − 2 Å s^{-1} for organic materials and 2 - 5 Å s^{-1} for aluminum, respectively. The current density, luminance versus driving voltage characteristics, and EL spectra were measured by a Keithley 2400 and a Konica Minolta CS2000 chromameter. EQEs were automatically estimated from the current density, brightness, and EL spectra, assuming a Lambertian distribution.

2. Synthetic procedures

All the reagents were purchased from the *Casmart Reagent* Platform or *Bidepharm* and used as received without further purification. The target molecules' intermediates were synthesized via a one-step, common palladium-catalyzed Buchwald-Hartwig reaction. The target molecules were synthesized via one-step common borylation reactions. The synthetic procedures are detailed below. All compounds show good solubility in toluene, chloroform, and THF, with Indo-tCzBN exhibiting slightly lower solubility due to the bulky t-Bu groups.

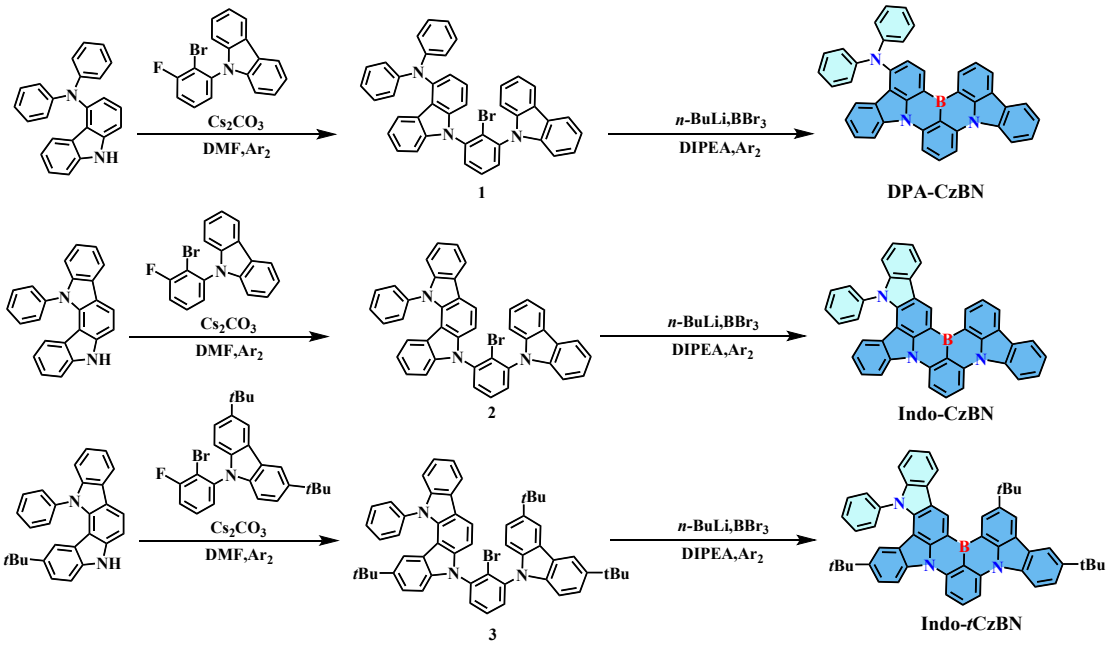

Scheme S1. Synthetic procedures of DPA-CzBN, Indo-CzBN, and Indo-*t*CzBN.

Synthesis of Compound 1: In a 250 mL flask charged with argon, a mixture of N, N-diphenyl-9H-carbazol-4-amine(6.68g,20.0 mmol), 9-(2-bromo-3-fluorophenyl)-9H-carbazole (6.8 g, 20.0 mmol), Cs $_2CO_3$(13.1 g, 40 mmol), and 120 mL N, N-dimethylformamide was vigorously stirred together at 11 0 ℃ overnight. The cooled mixture was filtered via diatomite and washed with dichloromethane. Af ter removed the organic solvent, the residual solid was further purified by flash column chromatogra phy on silica gel (eluting with petroleum ether/dichloromethane) to yield the pure product **1** as a w hite solid (9.79 g, 15 mmol, 75% yield).1H NMR (600 MHz, Chloroform-d) δ 8.18 (d, J = 7. 7 H z, 2H), 7.79 – 7.74 (m, 3H), 7.72 (d, J = 7.3 Hz, 1H), 7.46 (d, J = 7.5 Hz, 2H), 7.43 (d, J = 7.6 Hz, 1H), 7.38 – 7.31 (m, 3H), 7.21 (d, J = 7.5 Hz, 6H), 7.15 (d, J = 8.2 Hz, 5H), 7.06 (dd, J = 15.2, 7.1 Hz, 3H), 6.95 (t, J = 7.1 Hz, 2H).

Synthesis of Compound 2:In a 250 mL flask charged with argon, a mixture of 12-phenyl-5,12-dihy droindolo[3,2-a]carbazole(6.65g,20.0 mmol), 9-(2-bromo-3-fluorophenyl)-9H-carbazole (6.8g, 20.0 mmo

l), Cs2CO3(13.1 g, 40 mmol), and 120 mL N, N-dimethylformamide was vigorously stirred togethe r at 110 ℃ overnight. The cooled mixture was filtered via diatomite and washed with dichlorometh ane. After removed the organic solvent, the residual solid was further purified by flash column chro matography on silica gel (eluting with petroleum ether/dichloromethane) to yield the pure product **2** as a white solid (10.3 g, 16mmol, 79% yield).^{1}H NMR (600 MHz, Chloroform-d) δ 8.24 (d, J = 8. 4 Hz, 1H), 8.16 (d, J = 7.4 Hz, 3H), 7.80 – 7.76 (m, 1H), 7.73 (d, J = 7.8 Hz, 2H), 7.67 (s, 5H), 7.49 (t, J = 7.6 Hz, 1H), 7.45 (t, J = 7.6 Hz, 1H), 7.32 (ddt, J = 27.5, 17.3, 7.8 Hz, 6H), 7.25 (s, 1H), 7.20 (d, J = 8.1 Hz, 1H), 7.12 (d, J = 7.6 Hz, 2H), 6.83 (t, J = 7.6 Hz, 1H), 5.94 (d, J = 8.1 Hz, 1H).

Synthesis of Compound 3*:* In a 250 mL flask charged with argon, a mixture of 2-(tert-butyl)-12-ph enyl-5,12-dihydroindolo[3,2-a]carbazole(7.77g,20.0 mmol), 9-(2-bromo-3-fluorophenyl)-3,6-di-tert-butyl-9 H-carbazole (9.05g, 20.0 mmol), Cs2CO3(13.1 g, 40 mmol)and 120 mL N, N-Dimethylformamide were vigorously stirred together at 110 ℃ for overnight. The cooled mixture was filtered via diato mite and washed with dichloromethane. After removing the organic solvent, the residual solid was f urther purified by flash column chromatography on silica gel (eluted with petroleum ether/dichlorom ethane) to yield the pure product 3 as a yellow solid (11.6 g, 14 mmol, 71% yield). 1H NMR (600 MHz, Chloroform-d) δ 8.24 (dd, J = 8.4, 1.9 Hz, 1H), 8.17 (dd, J = 12.6, 4.6 Hz, 3H), 7.79 – 7.7 3 (m, 1H), 7.69 (h, J = 8.1, 7.5 Hz, 6H), 7.62 (dt, J = 8.5, 4.2 Hz, 1H), 7.55 (dd, J = 8.5, 2.1 Hz, 1H), 7.51 (d, J = 8.4 Hz, 1H), 7.41 (d, J = 8.4 Hz, 1H), 7.37 – 7.30 (m, 3H), 7.20 (dd, J = 8.6, 1.9 Hz, 1H), 7.16 – 7.12 (m, 2H), 7.10 (dd, J = 8.5, 1.9 Hz, 1H), 6.66 (s, 1H), 1.49 (d, J = 8.6 Hz, 18H), 1.14 (s, 9H).

Synthesis of Target Compound DPA-CzBN*:* In a 120 mL sealed tube charged with argon, substrate s 1 (1.30g, 2.0 mmol) and 15 mL N, N-Diisopropylethylamine (DIPEA) were added. After adding boron bromide (5.00 g, 20.0 mmol), the tube was sealed and stirred at 220 °C for 48 h. After cool ing to room temperature, the reaction was quenched by slowly adding ethanol (5.0 mL) under an ic e bath. The organic solvent was concentrated under vacuum conditions. The residual solid was furt her purified by flash column chromatography on silica gel (eluting with petroleum ether/dichloromet hane) to yield the pure product DPA-CzBN as a bright yellow solid (0.86 g, 1.4mmol, 74% yield). 1H NMR (600 MHz, Chloroform-d) δ 8.93 (d, J = 7.9 Hz, 1H), 8.89 (d, J = 7.4 Hz, 1H), 8.57 – 8.42 (m, 2H), 8.36 (t, J = 7.4 Hz, 3H), 8.24 (d, J = 7.5 Hz, 1H), 8.00 (t, J = 8.2 Hz, 1H), 7.80 (d, J = 7.9 Hz, 1H), 7.63 (dt, J = 16.9, 7.6 Hz, 2H), 7.50 (t, J = 7.8 Hz, 1H), 7.44 (d, J = 7.7 Hz, 1H), 7.34 (d, J = 8.0 Hz, 1H), 7.28 (d, J = 8.1 Hz, 3H), 7.22 (d, J = 8.5 Hz, 4H), 7.15 (q, J = 7.7 Hz, 2H), 7.03 (t, J = 7.4 Hz, 2H).

Synthesis of Target Compound Indo-CzBN*:* The synthesis of Compound Indo-CzBN followed the i dentical methodology used for Compound DPA-CzBN, The resulting product was a bright green soli d with a yield of 69%.1H NMR (600 MHz, Chloroform-d) δ 9.74 (s, 1H), 9.15 (d, J = 7.4 Hz, 1 H), 8.51 (t, J = 10.7 Hz, 2H), 8.46 (s, 1H), 8.39 (d, J = 21.6 Hz, 3H), 8.26 (s, 1H), 7.99 (s, 1H),

7.78 (s, 1H), 7.70 (s, 5H), 7.63 (s, 1H), 7.47 (s, 3H), 7.42 (s, 1H), 7.38 (s, 1H), 6.94 (s, 1H), 6.09 (d, J = 8.0 Hz, 1H).

Synthesis of Target Compound Indo-tCzBN: The synthesis of Compound Indo-tCzBN followed the identical methodology used for Compound DPA-CzBN, The resulting product was a bright yellow solid with a yield of 70%.1H NMR (600 MHz, Chloroform-d) δ 9.81 (s, 1H), 9.27 (s, 1H), 8.50 (s, 2H), 8.38 (dd, J = 19.7, 10.3 Hz, 4H), 8.29 (s, 1H), 8.03 – 7.96 (m, 1H), 7.73 (t, J = 11.2 Hz, 6H), 7.46 (s, 3H), 7.41 (d, J = 7.2 Hz, 1H), 6.82 (s, 1H), 1.76 (s, 9H), 1.55 (s, 9H), 1.17 (s, 9H).

3. Thermo-stability Properties

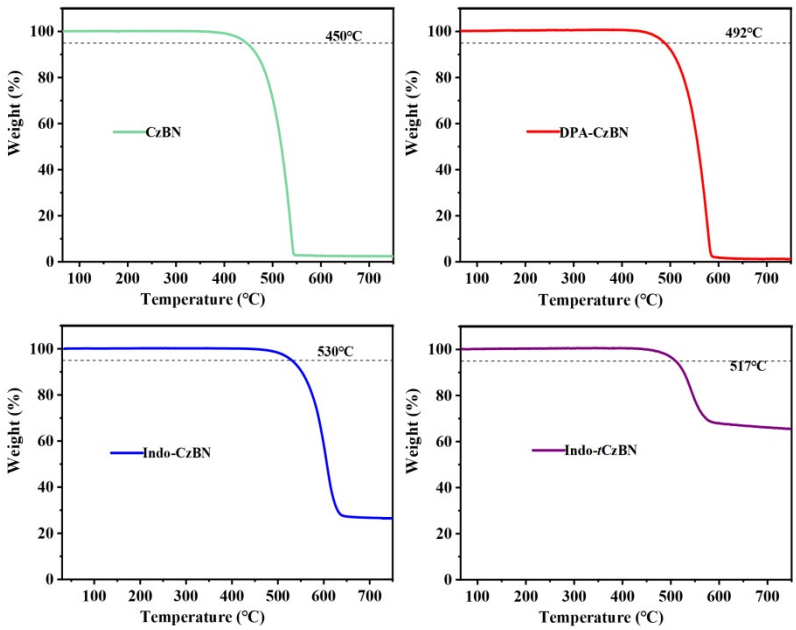

Figure S1. The thermogravimetric analysis curves of (A) CzBN, (B) DPA-CzBN, (C) Indo-CzBN, and (D) Indo-*t*CzBN, respectively.

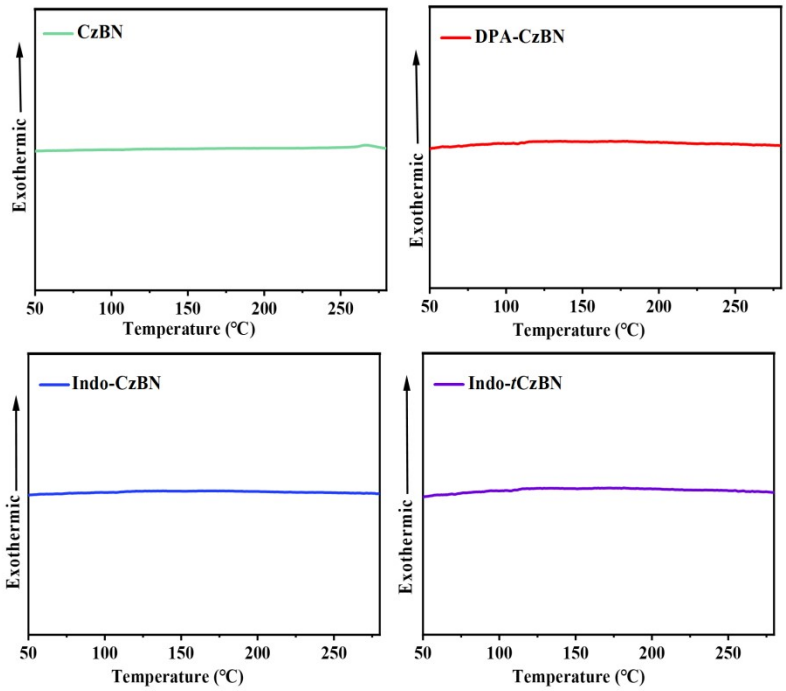

Figure S2. The differential scanning calorimetry curves of (A) CzBN, (B) DPA-CzBN, (C) Indo-CzBN, and (D) Indo-tCzBN, respectively.

4. Computational Data

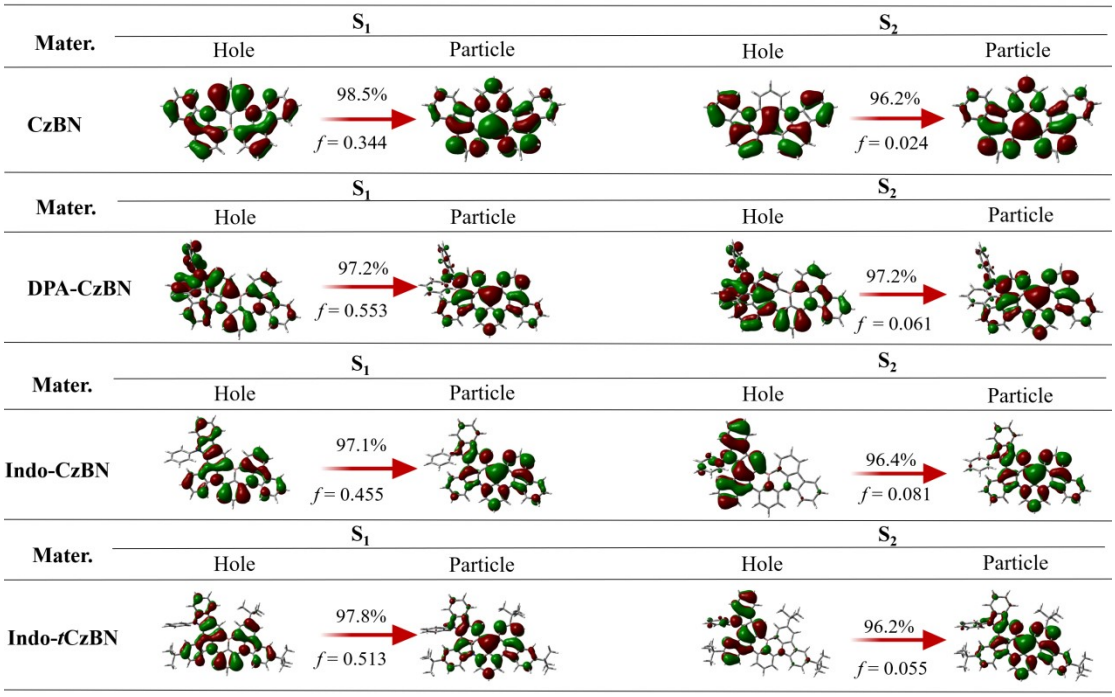

Figure S3. The natural transition orbits (NTOs) of CzBN, DPA-CzBN, Indo-CzBN, and Indo-*t*CzBN in S_1 and S_2 states.

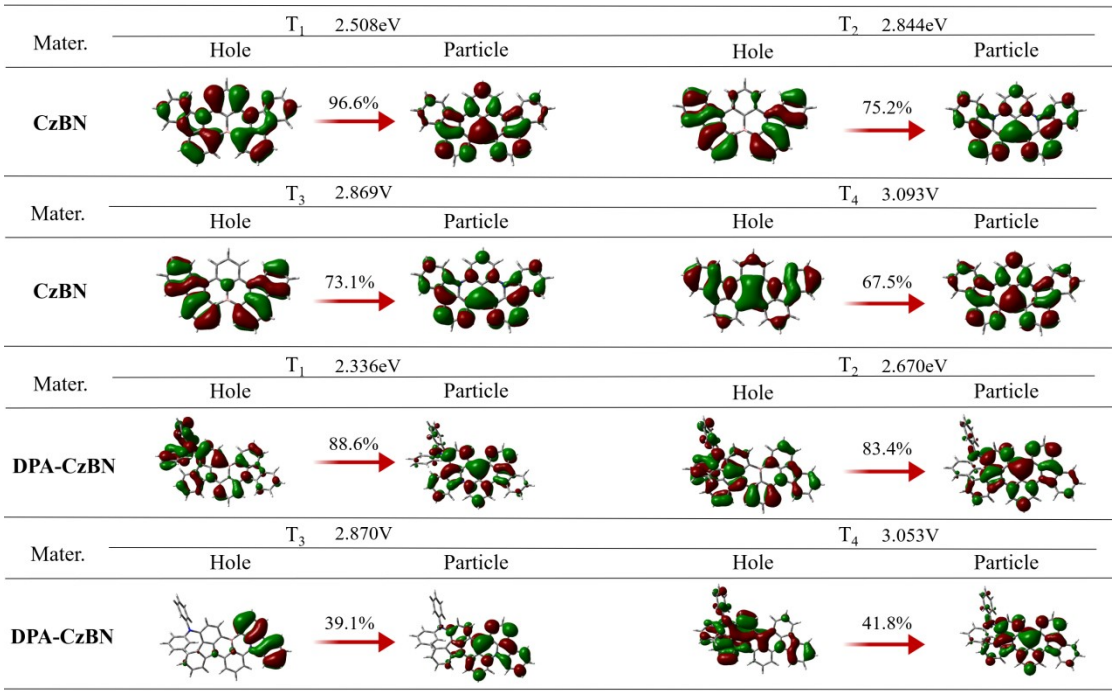

Figure S4. The natural transition orbits (NTOs) of CzBN and DPA-CzBN in T_n states ($n \leq 4$).

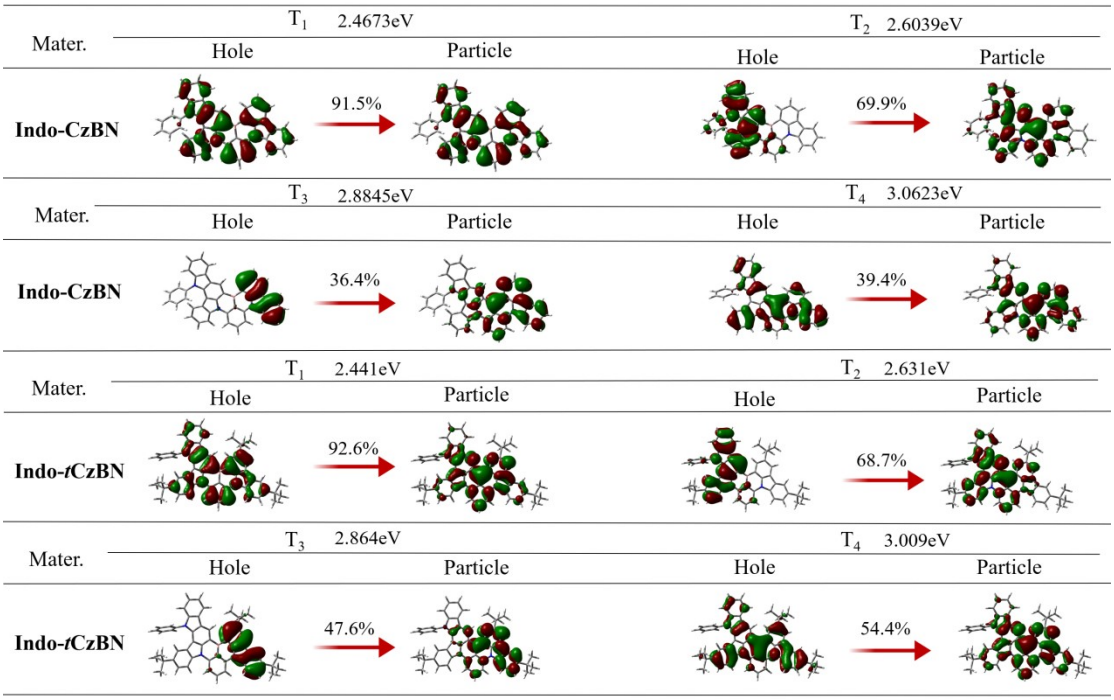

Figure S5. The natural transition orbits (NTOs) of Indo-CzBN and Indo-*t*CzBN in T_n states ($n \leq 4$).

Compound	CzBN	DPA-CzBN	Indo-CzBN	Indo-*t*CzBN
Structure	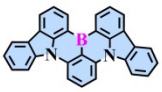	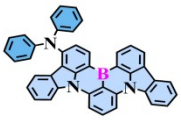	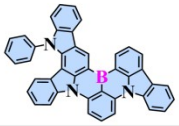	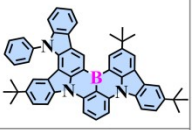
RMSD	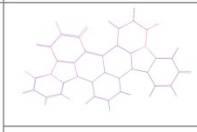	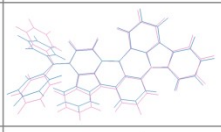	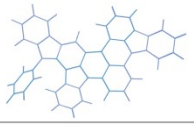	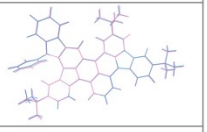
	0.0579 Å	0.8229 Å	0.0571 Å	0.1703 Å

Figure S6. The calculated root-mean-square deviations (RMSDs) of CzBN, DPA-CzBN, Indo-CzBN, and Indo-*t*CzBN, respectively.

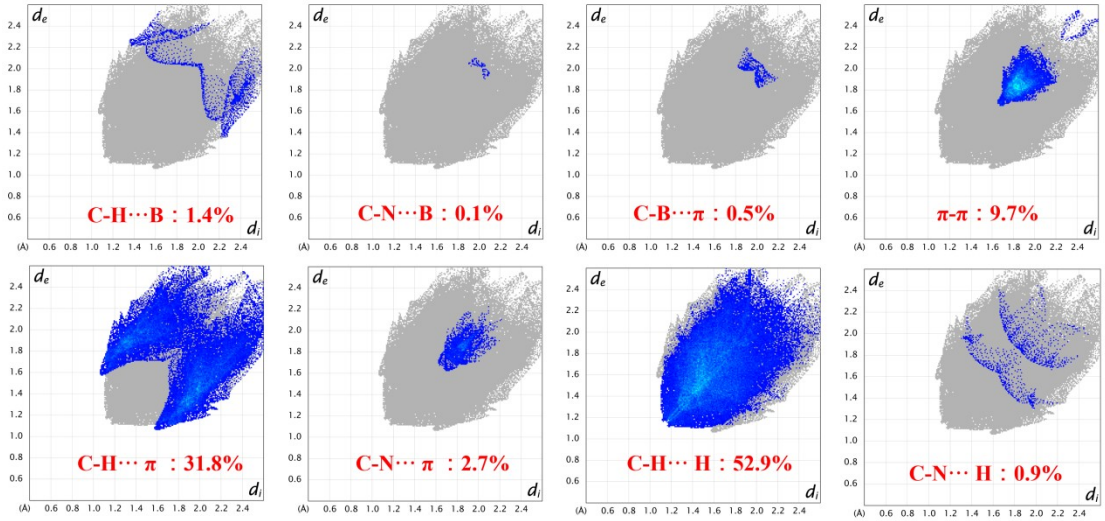

Figure S7. The primary intermolecular π-π interactions in the DPA-CzBN crystal.

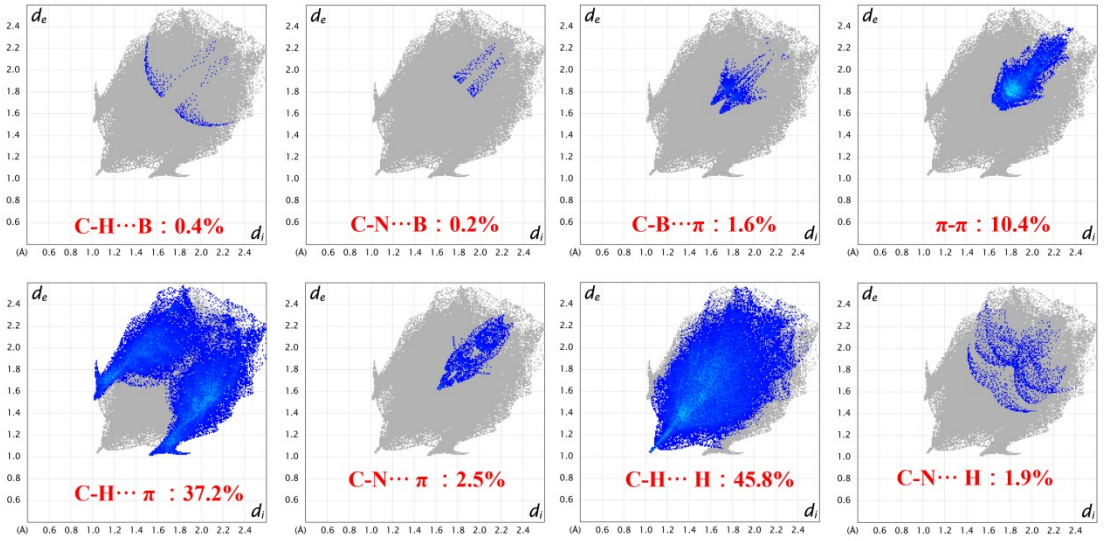

Figure S8. The primary intermolecular π-π interactions in the Indo-CzBN crystal.

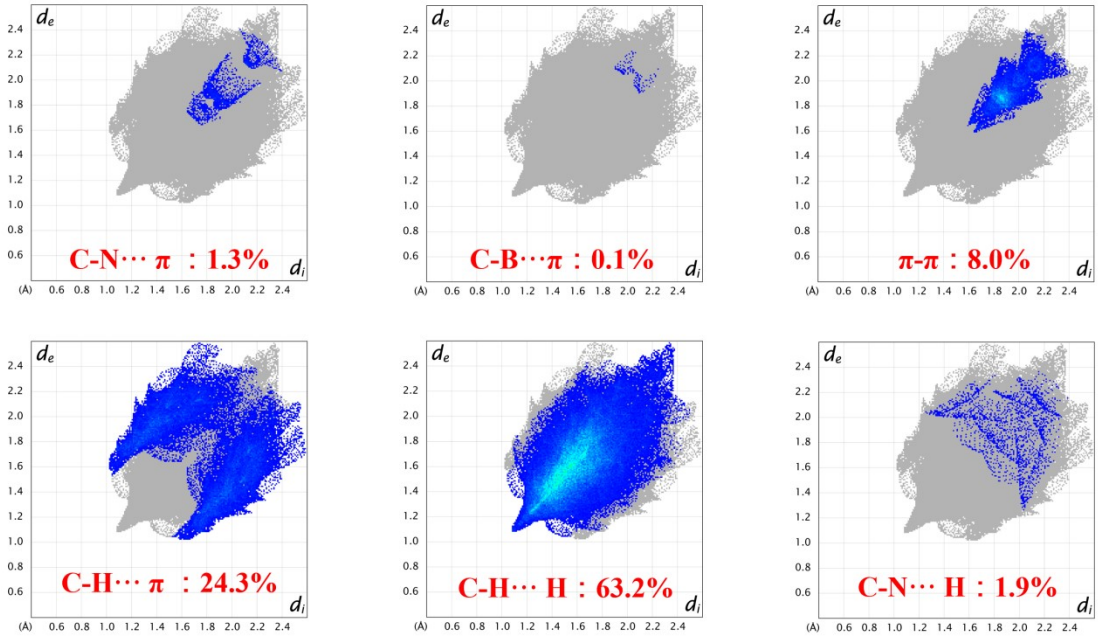

Figure S9. The primary intermolecular π-π interactions in the Indo-tCzBN crystal.

5. Photophysical properties

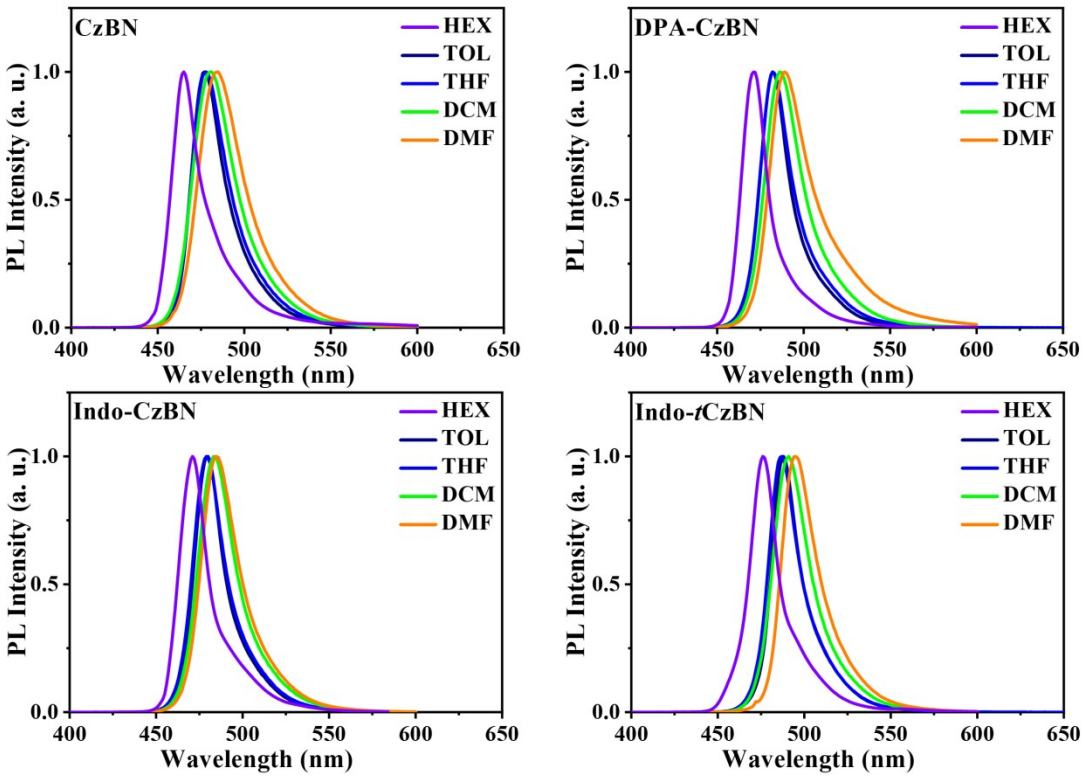

Figure S10. Solvation effect: the PL spectra of CzBN, DPA-CzBN, Indo-CzBN, and Indo-tCzBN in different solvents. Herein, HEX, TOL, THF, DCM, and DMF denote the solvents of *n*-hexane, toluene, tetrahydrofuran, 1,4-dioxane, and *N*, *N*-dimethylformamide, respectively.

Table S1. Summary of photophysical properties of CzBN, DPA-CzBN, Indo-CzBN, and Indo-tCzBN, respectively.

Emitters	T_d[a)]	λ_{abs}[b)]	λ_{em}[c)]	HOMO[d)]	LUMO[d)]	S_1[e)]	T_1[e)]	ΔE_{ST}[e)]
	[°C]	[nm]	[nm]	[eV]	[eV]	[eV]	[eV]	[eV]
CzBN	450	458	477	-5.2	-2.6	2.59	2.46	0.13
DPA-CzBN	492	467	482	-5.4	-2.6	2.51	2.34	0.17
Indo-CzBN	530	465	480	-5.4	-2.6	2.55	2.44	0.11
Indo-*t*CzBN	517	472	488	-5.4	-2.5	2.53	2.48	0.04

[a)] decomposition temperature (T_d) (5% weight loss); [b)] UV-vis absorption in toluene solutions at room temperature; [c)] PL peaks in dilute toluene solution at room temperature; [d)] experimental HOMO/LUMO determined from cyclic voltammetry and calculated of the bandgap in UV-vis absorption spectra; [d)] S_1, T_1, and ΔE_{ST}s were evaluated in dilute toluene at 77 K.

Table S2. The UV-vis characteristics of CzBN, DPA-CzBN, Indo-CzBN, and Indo-*t*CzBN in different solvents.

Emitters	λ_{em} (nm)/FWHM (nm)				
	Hex	Tol	THF	DCM	DMF
CzBN	465/20	477/23	478/25	481/29	485/31
DPA-CzBN	471/18	482/21	482/22	486/26	489/29
Indo-CzBN	471/19	480/21	479/22	484/25	485/26
Indo-*t*CzBN	476/18	488/19	487/21	491/25	495/25

Table S3. Photo-physical properties of 3 wt.% CzBN, DPA-CzBN, Indo-CzBN, and Indo-*t*CzBN in *doped* films deposited by vacuum evaporation were measured at room temperature.The PLQY is an average of three measurements with a standard deviation of ±1.2%.

Emitters	Φ_{PL}	Φ_{PF}	Φ_{TADF}	τ_{PF}	τ_{DF}	k_r^s	k_{isc}^s	k_{risc}^s	k_{TADF}
	[%]	[%]	[%]	[ns]	[μs]	[$10^7 s^{-1}$]	[$10^7 s^{-1}$]	[$10^4 s^{-1}$]	[$10^4 s^{-1}$]
CzBN	80.2	59.4	20.8	8.44	75.41	7.0	4.8	1.1	0.68
DPA-CzBN	81.2	69.3	11.9	4.01	340.9	17.0	7.6	0.16	0.11
Indo-CzBN	85.7	74.4	11.3	4.85	61.9	15.0	5.3	0.9	0.71
Indo-*t*CzBN	97.5	78.2	19.3	4.14	56.0	19.0	5.3	2.0	1.6

6. Crystal properties

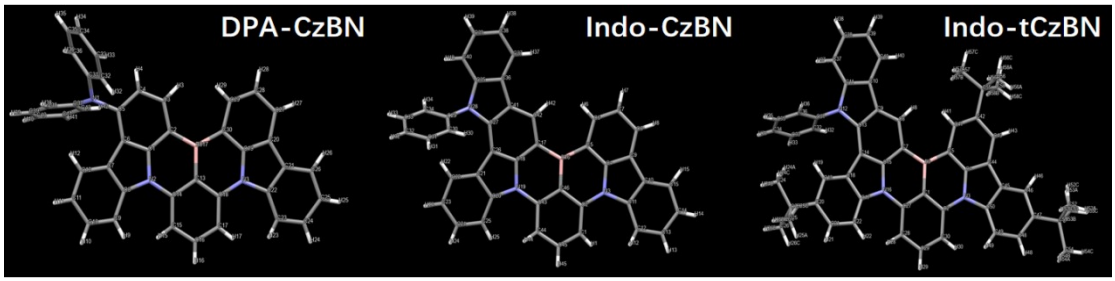

Figure S11. The single-crystal of DPA-CzBN, Indo-CzBN, and Indo-tCzBN, respectively.

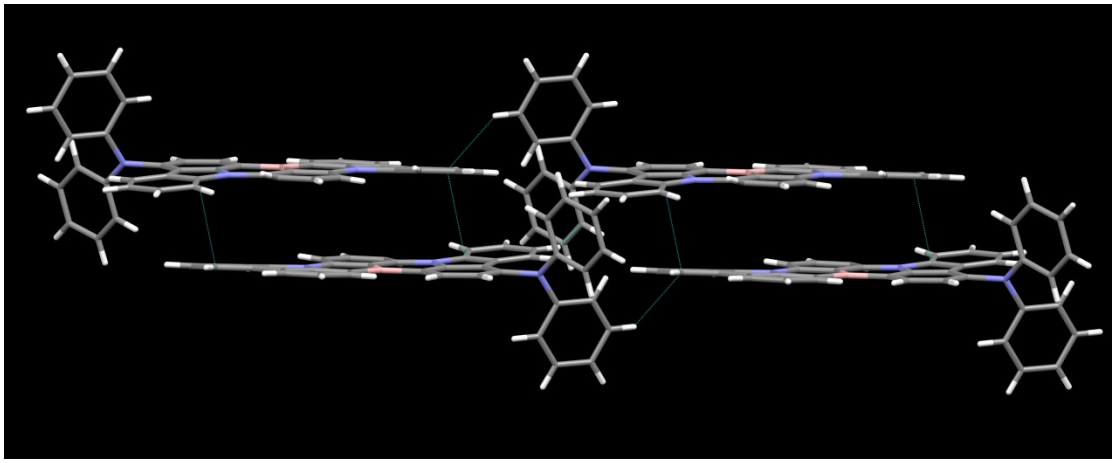

Figure S12. Packing modes of DPA-CzBN crystals.

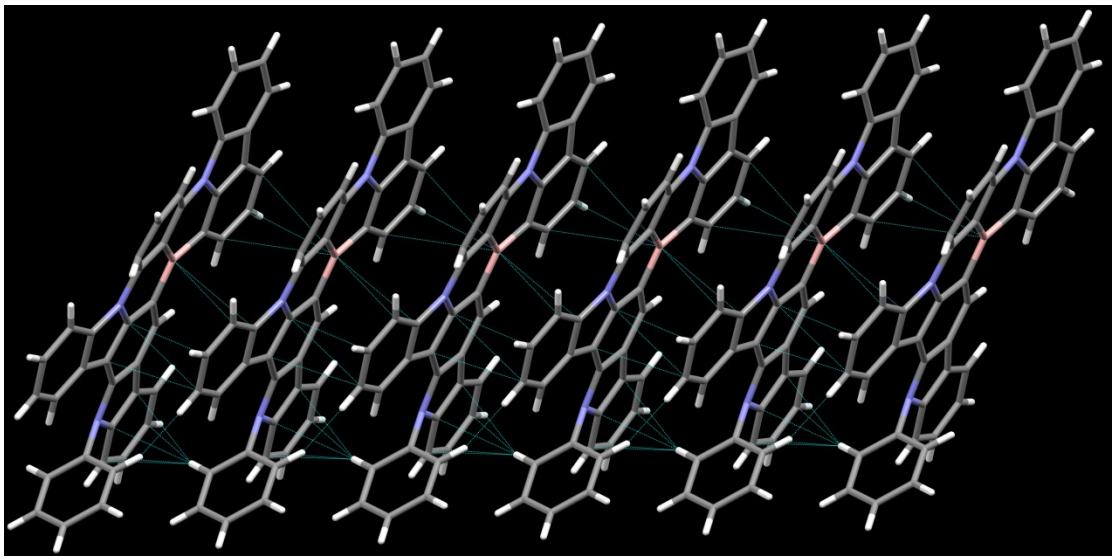

Figure S13. Packing modes of Indo-CzBN crystals.

.

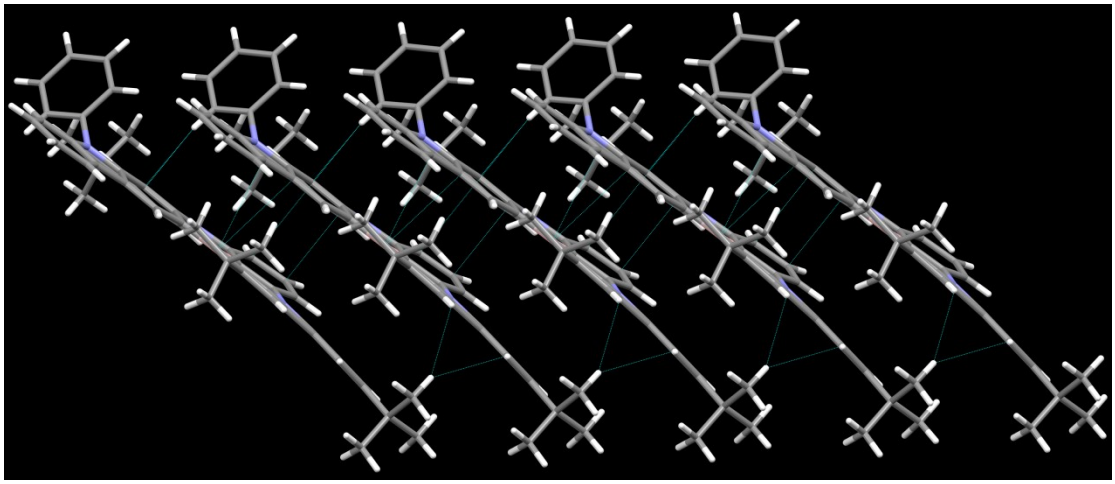

Figure S14. Packing modes of Indo-*t*CzBN crystals.

Table S4. Crystal data and structure refinement for DPA-CzBN, Indo-CzBN, and Indo-*t*CzBN.

Identification code	DPA-CzBN	Indo-CzBN	Indo-tCzBN
Empirical formula	$C_{42}H_{26}BN_3$	$C_{42}H_{24}BN_3$	$C_{54}H_{48}BN_3$
Formula weight	583.47	581.45	749.76
Temperature/K	170	170	130
Crystal system	triclinic	monoclinic	monoclinic
Space group	P-1	P2/c	$P2_1/c$
a/Å	9.6464(3)	35.034(3)	5.7410(4)
b/Å	13.1116(4)	5.3550(5)	20.0142(14)
c/Å	13.2323(5)	33.077(3)	34.391(3)
α/°	60.773(2)	90	90
β/°	76.190(2)	117.999(5)	91.849(5)
γ/°	83.758(2)	90	90
Volume/Å^3, z	1418.27(9)	5479.1(9)	3949.5(5)
Density/g cm^{-3}	1.366	1.410	1.261
μ/mm^{-1}	0.614	0.635	0.552
Z	2	8	4
CCDC	2485480	2485481	2485482

7. Electrochemical measurements

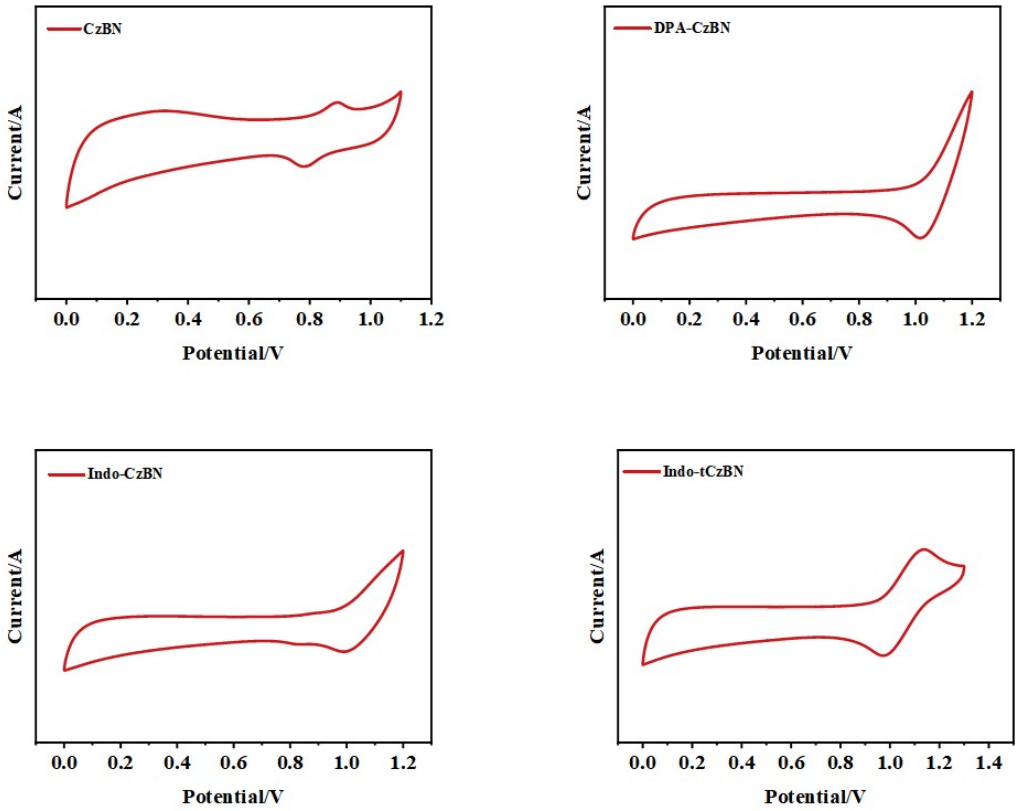

Figure S15. Cyclic voltammetry measurements of CzBN, DPA-CzBN, Indo-CzBN, and Indo-*t*CzBN, respectively.

8. OLED characterization

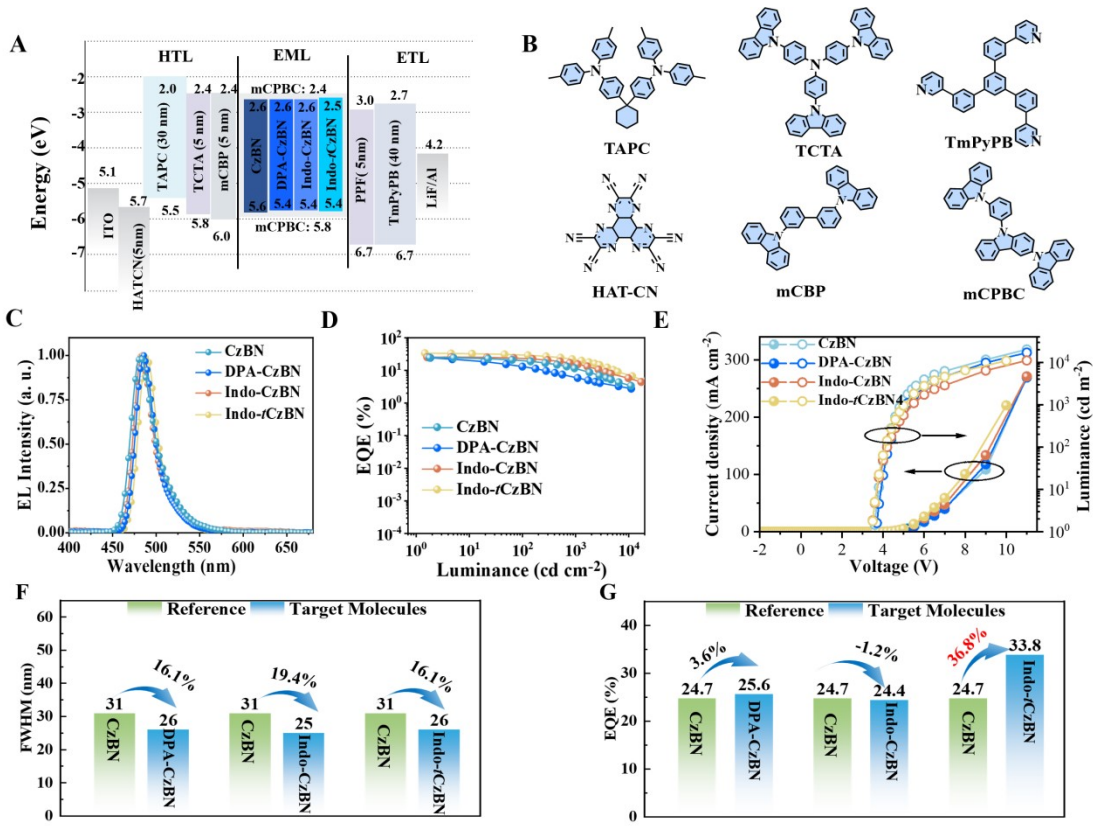

Figure S16. (A) The device architecture and energy diagram, (B) the functional layer materials used in these OLEDs, (C) the EL spectra, (D) EQE-luminance curves, (E) current density–voltage–luminance curves, (F) comparison chart of FWHM values, and (G) comparison chart of EQE_{max} values of non-sensitized OLEDs based on CzBN, DPA-CzBN, Indo-CzBN, and Indo-*t*CzBN with a doping concentration of 1 wt.%.

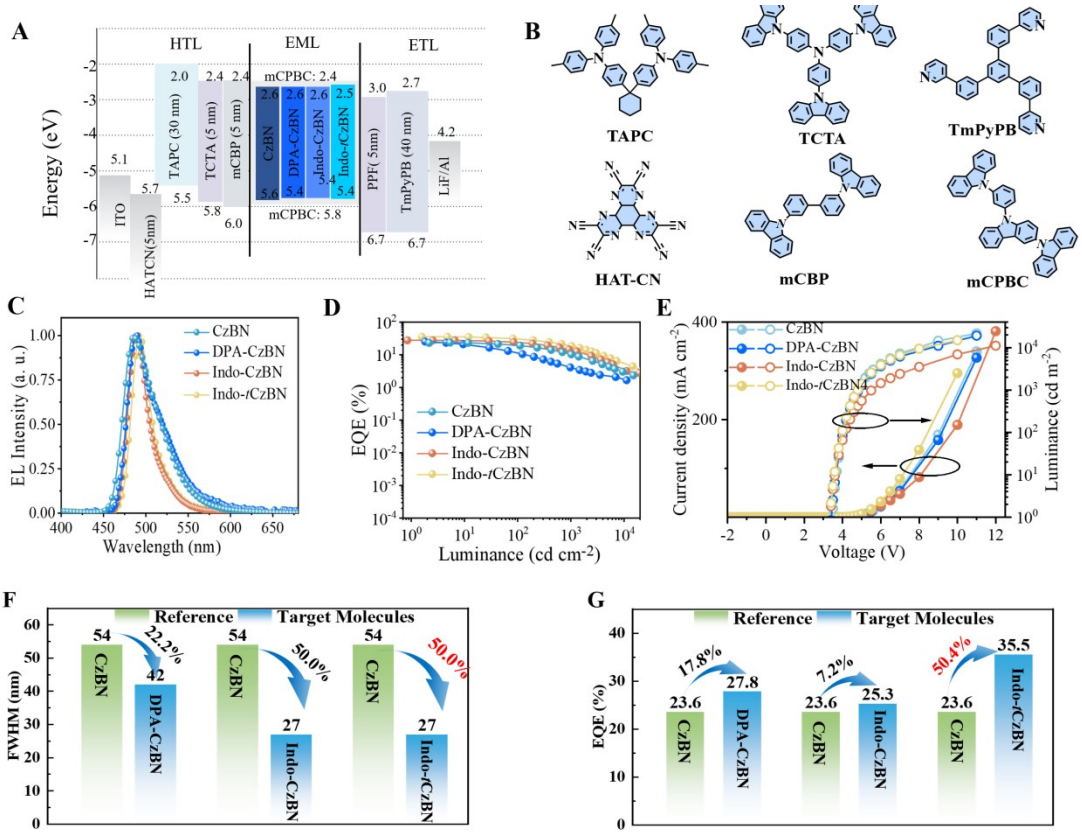

Figure S17. (A) The device architecture and energy diagram, (B) the functional layer materials used in these OLEDs, (C) the EL spectra, (D) EQE-luminance curves, (E) current density–voltage–luminance curves, (F) comparison chart of FWHM values, and (G) comparison chart of EQE_{max} values of non-sensitized OLEDs based on CzBN, DPA-CzBN, Indo-CzBN, and Indo-*t*CzBN with a doping concentration of 5 wt.%.

Table S5. EL performance of interlayer HF-OLEDs based on CzBN, DPA-CzBN, Indo-CzBN, and Indo-*t*CzBNBN, respectively, with a doping concentration of 3 wt.%.

Emitter	*Dop.* [%]	V_{on} [V]	*CE*/*PE*/EQE (cd A^{-1})/(lm W^{-1})/(%)	FWHM (nm)	L_{max} (cd m^{-2})	λ_{EL} (nm)	CIE (x, y)
CzBN	3	3.2	46.9/45.4/25.0	36	484	14190	(0.11,0.35)
DPA-CzBN	3	3.1	52.6/53.3/30.2	28	486	16160	(0.10,0.33)
Indo-CzBN	3	3.1	46.8/47.5/28.1	27	486	13130	(0.09,0.33)
*Indo-t*CzBN	3	3.1	69.5/70.4/39.0	26	490	23540	(0.09,0.38)

Table S6. Summary of OLEDs based on MR-TADF emitters with a single BN molecular structure.

Emitter	Ref	λ (nm)	FWHM (nm)	EQE_{max} (%)	CIE(x, y)
CzBN	**This work**	482	31	24.7	(0.10,0.29)
		486	46	23.7	(0.13,0.43)
		490	54	23.6	(0.14,0.48)
DPA-CzBN	This work	484	36	25.0	(0.11,0.35)
		486	25	24.4	(0.09,0.32)
		488	27	25.5	(0.09,0.37)
		490	27	25.3	(0.09,0.40)
Indo-CzBN	This work	486	27	28.1	(0.09,0.33)
		484	26	25.6	(0.09,0.30)
		486	31	27.1	(0.11,0.41)
		490	42	27.8	(0.14,0.48)
Indo-tCzBN	This work	486	28	30.2	(0.10,0.33)
		490	26	33.8	(0.08,0.37)
		490	26	37.4	(0.08,0.44)
		492	27	35.5	(0.08,0.46)
		490	26	39.0	(0.09,0.38)
m-Cz-DABNA	*Angew. Chem. Int. Ed.* **2025,** e202510190	456	25	23.0	(0.14, 0.06)
tBu-Cz-DABNA		467	27	28.5	(0.13, 0.13)
D-BNNGe	*Adv. Optical Mater.* **2024,** *12*, 2401033	495	26	31.0	(0.09,0.51)
D-BNOGe		465	41	15.5	(0.13,0.17)
D-BNSGe		488	32	20.7	(0.11,0.37)
mono-mx-CzDABNA	*Adv. Funct. Mater.* **2023**, *33*, 2213461	481	48	21.4	(0.13, 0.24)
tri-mx-CzDABNA		472	34	26.9	(0.13, 0.19)
p/m-**Cz-BCzBN**	*Chem. Sci.***, 2025,** *16*, 3904-3915	492	29	27.8	(0.10, 0.45)
tCzAzBN	*Mater. Horiz.*, **2025**,*12*, 9737-9748	474	28	18.7	(0.11, 0.17)
tCzPAzBN		473	25	35.2	(0.12, 0.16)
tCzPAzBN		473	29	40.1	(0.15, 0.25)
BN-CP1	*Adv. Mater.*, **2022**, 34, 2106954	496	25	40.0	(0.09,0.50)
BN-CP2		497	26	36.4	(0.10,0.53)
S-Cz-BN		494	31	28.8	(0.10,0.46)

D-Cz-BN	*Angew. Chem., Int. Ed.,* **2022**, 61, e202113206	488	24	37.2	(0.11,0.43)
D-*p*−1-PCzBN	*Adv. Opt. Mater.*, **2023**, *11*, 2203002	496	26	33.9	(0.08,0.52)
SF1BN	*Angew. Chem., Int. Ed.*, **2022**, *61*, e202201886	492	27	35.9	(0.07,0.47)
SF3BN		496	30	32.2	(0.09,0.51)
m-PCz–BNCz	*Adv. Mater.,* **2023**, *35,* 2205166	504	29	36.8	(0.11, 0.61)
m-DPAcP–BNCz		496	28	42.0	(0.09, 0.54)
m-BN–BNCz		492	28	35.0	(0.09, 0.48)
m-SF–BNCz		496	28	41.1	(0.09, 0.53)
tDPAC-BN	*Chem. Eng. J.*, **2022**, *431*, 133221	460	28	21.6	(0.13,0.09)
tDMAC-BN		472	34	22.3	(0.11,0.18)
BNCz-NPO	*Nat. Commun*., **2024**, *15*, 6175	480	26	37.6	(0.11,0.18)
BNCz-NPS		476	30	32.2	(0.13,0.18)

9. NMR Spectra

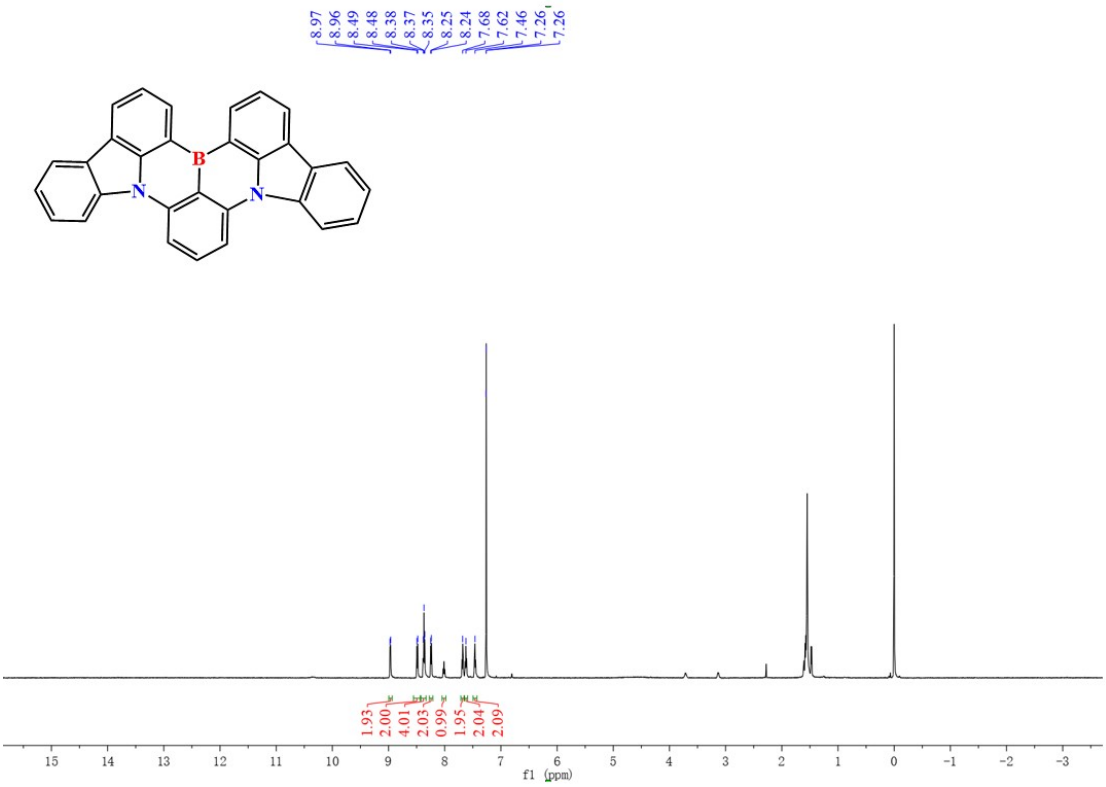

Figure S18. ^{1}H NMR spectrum of **CzBN** in $CDCl_3$ solvent.

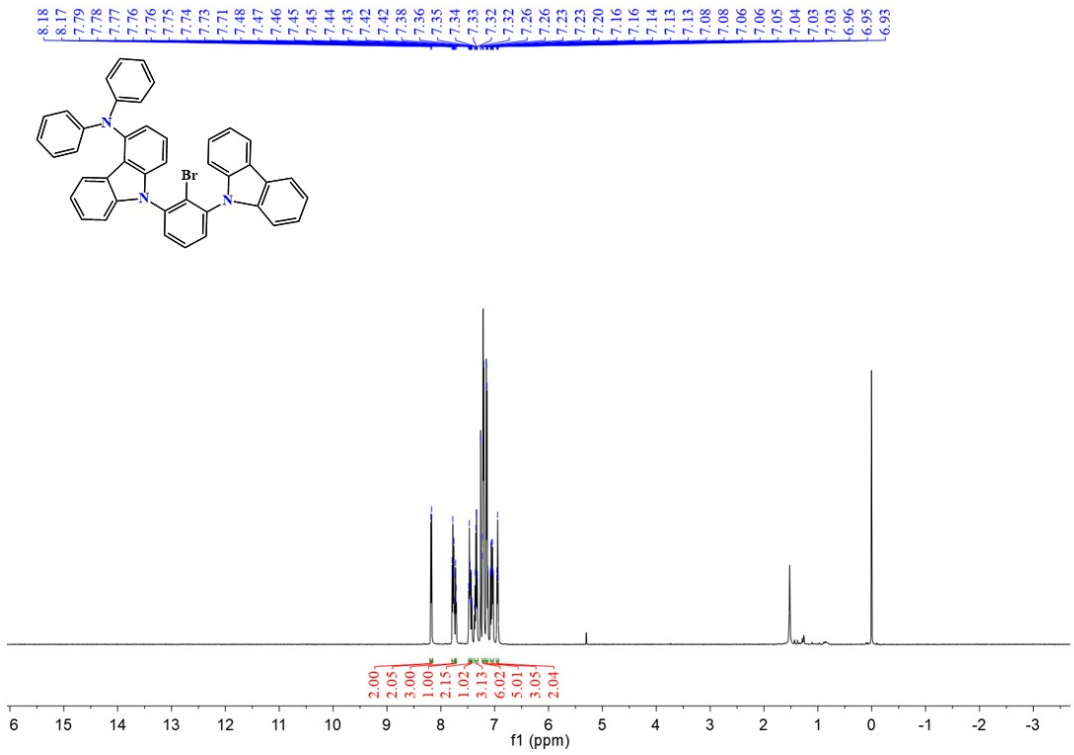

Figure S19. ^{1}H NMR spectrum of compound **1** in $CDCl_3$ solvent.

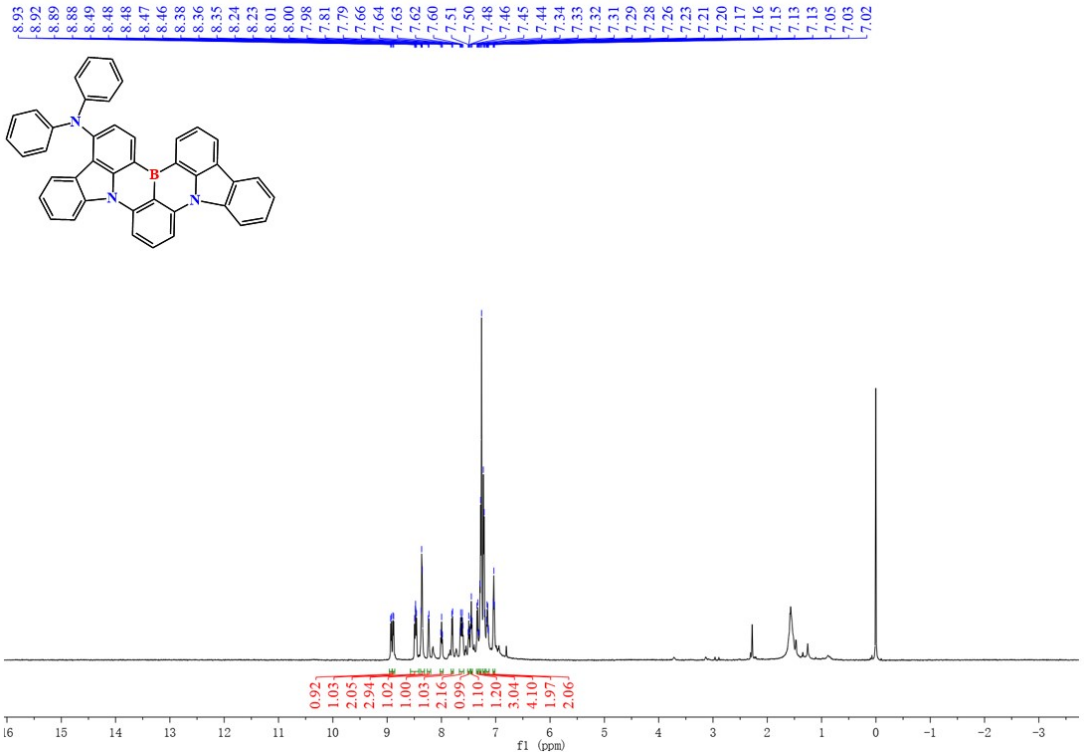

Figure S20. ^{1}H NMR spectrum of **DPA-CzBN** in $CDCl_3$ solvent.

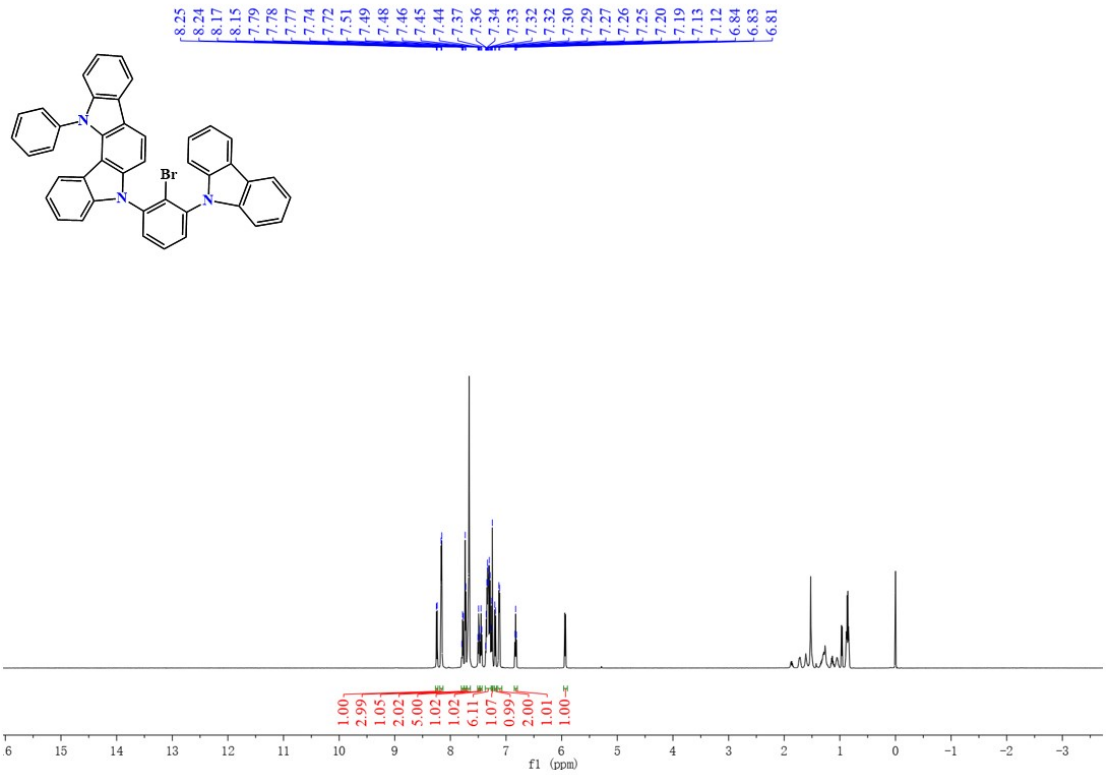

Figure S21. ^{1}H NMR spectrum of compound **2** in $CDCl_3$ solvent.

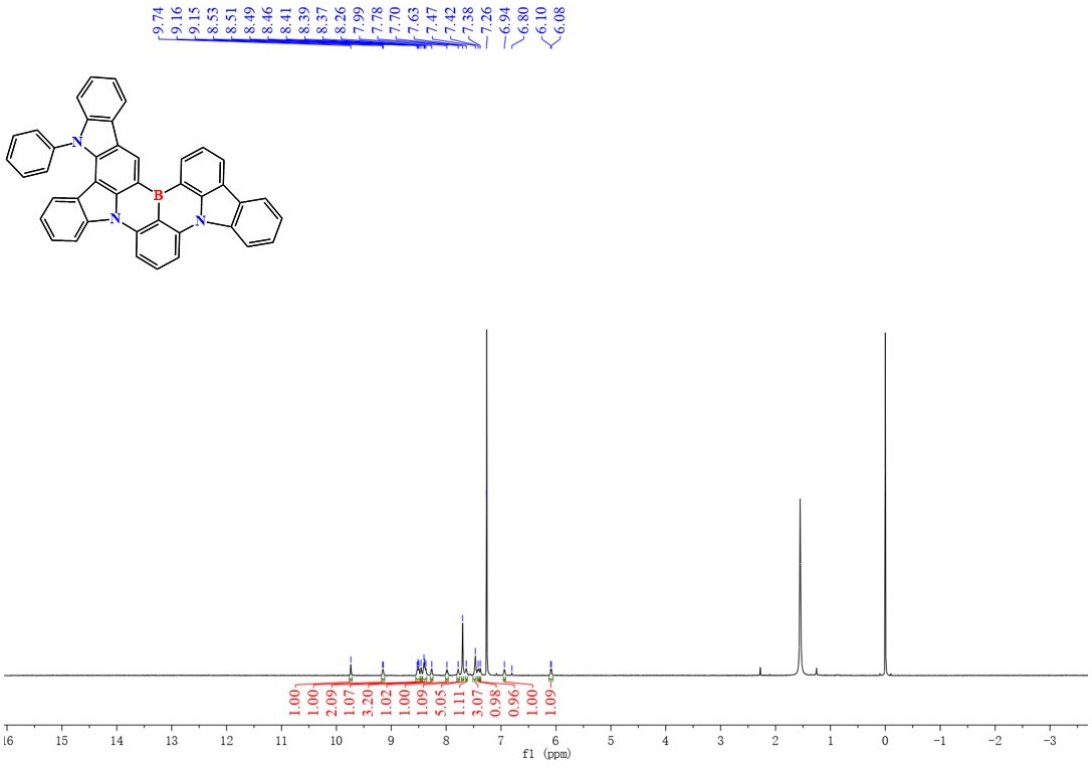

Figure S22. ^{1}H NMR spectrum of **Indo-CzBN** in $CDCl_3$ solvent.

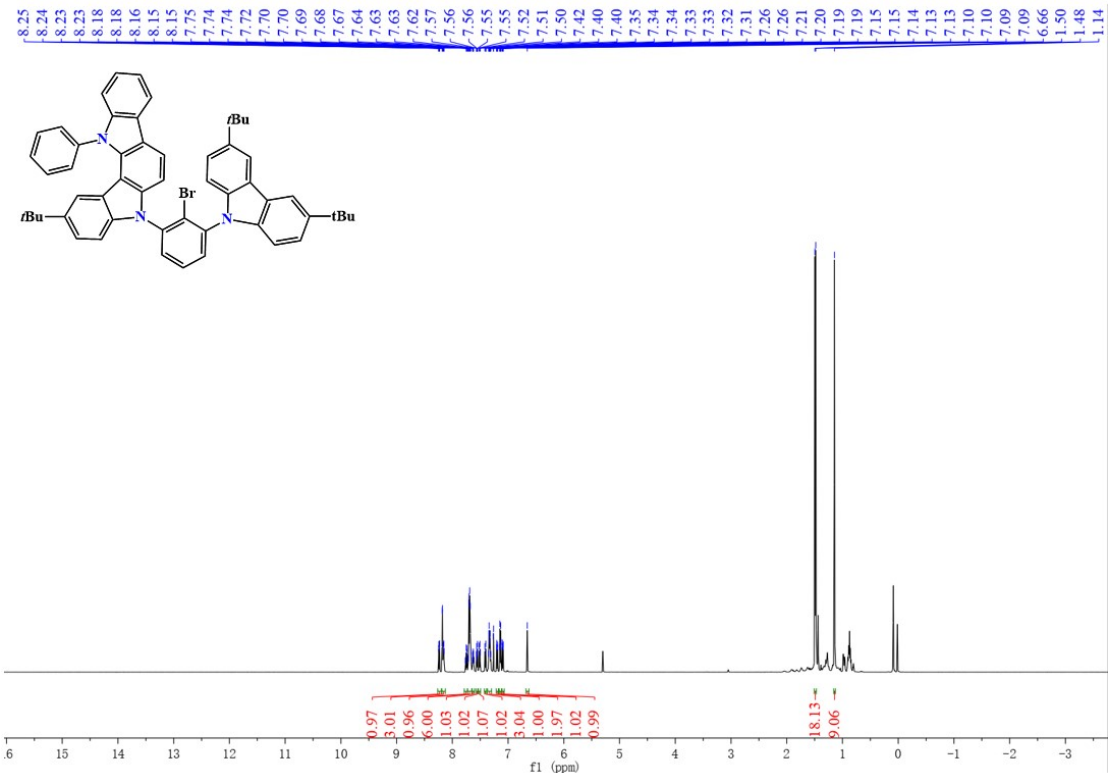

Figure S23. ^{1}H NMR spectrum of compound **3** in $CDCl_3$ solvent.

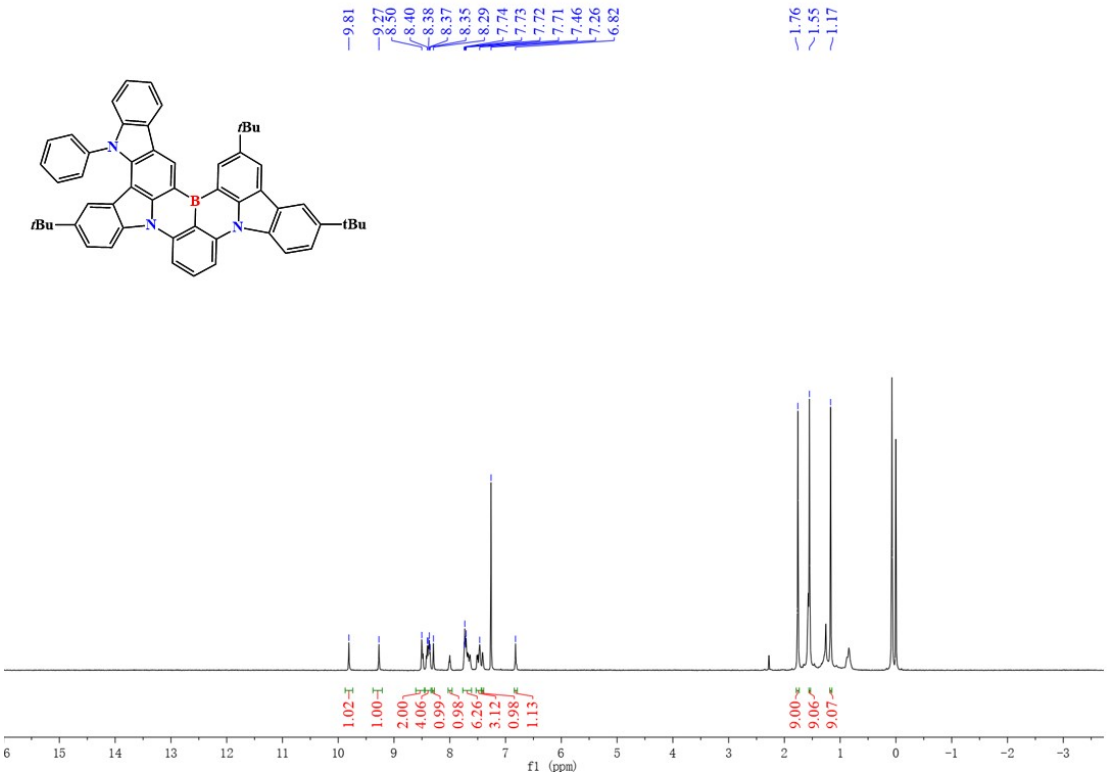

Figure S24. ^{1}H NMR spectrum of **Indo-tCzBN** in $CDCl_3$ solvent.

10. Mass spectra

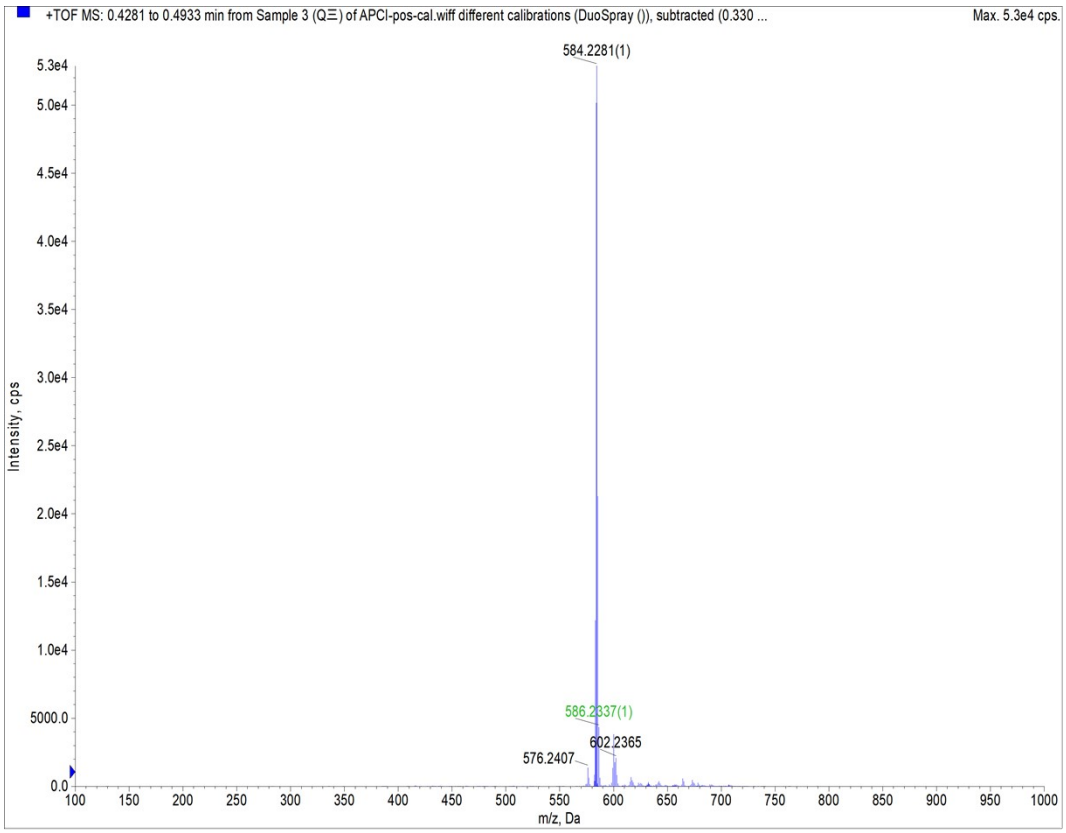

Figure S25. Mass spectra of **DPA-CzBN** in $CHCl_2$ solvent

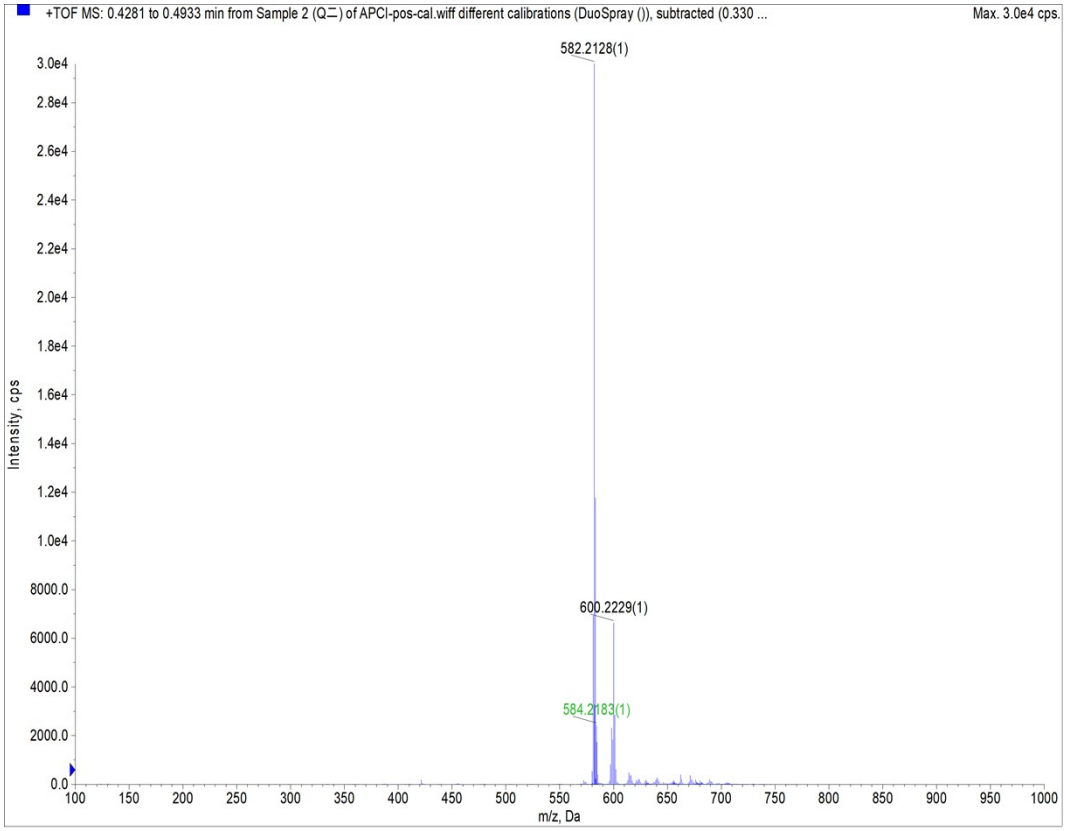

Figure S26. Mass spectra of **Indo-CzBN** in $CHCl_2$ solvent

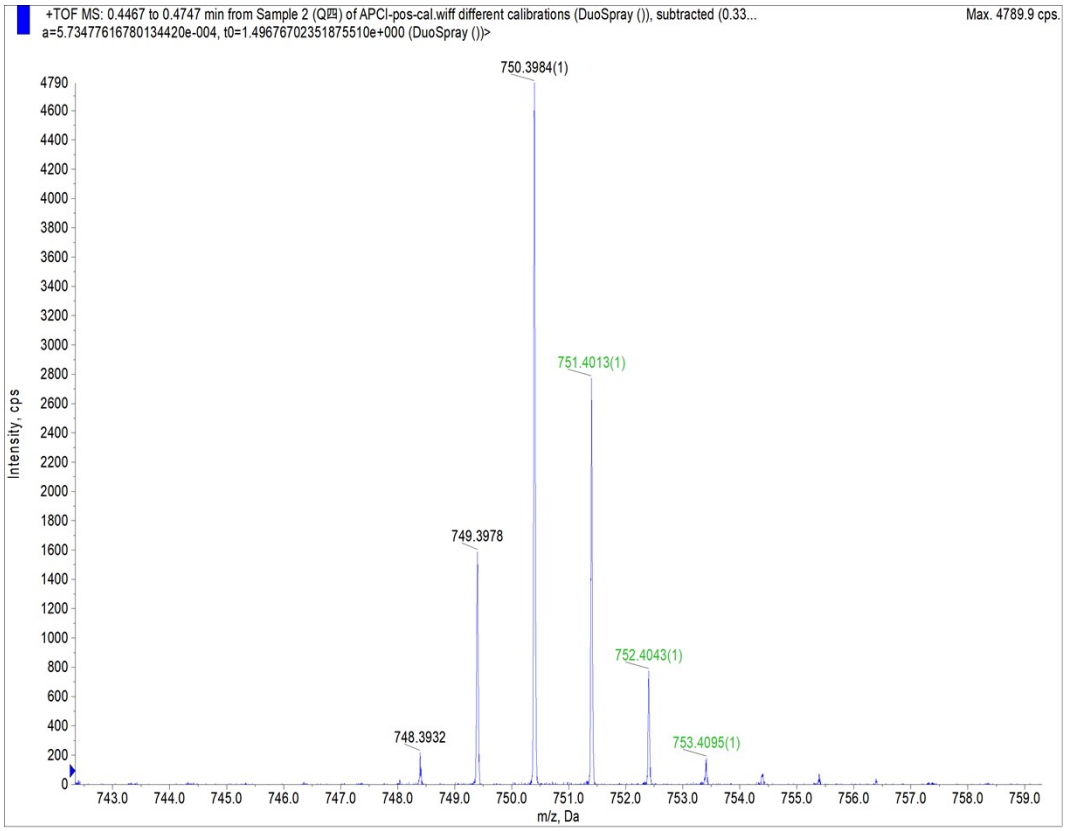

Figure S27. Mass spectra of **Indo-tCzBN** in $CHCl_2$ solvent

11. Reference

[1] M. J. Frisch, G. W. Trucks, H. B. Schlegel, G. E. Scuseria, M. A. Robb, J. R. Cheeseman, G. Scalmani, V. Barone, G. A. Petersson, H. Nakatsuji, X. Li, M. Caricato, A. V. Marenich, J. Bloino, B. G. Janesko, R. Gomperts, B. Mennucci, H. P. Hratchian, J. V. Ortiz, A. F. Izmaylov, J. L. Sonnenberg, Williams, F. Ding, F. Lipparini, F. Egidi, J. Goings, B. Peng, A. Petrone, T. Henderson, D. Ranasinghe, V. G. Zakrzewski, J. Gao, N. Rega, G. Zheng, W. Liang, M. Hada, M. Ehara, K. Toyota, R. Fukuda, J. Hasegawa, M. Ishida, T. Nakajima, Y. Honda, O. Kitao, H. Nakai, T. Vreven, K. Throssell, J. A. Montgomery Jr., J. E. Peralta, F. Ogliaro, M. J. Bearpark, J. J. Heyd, E. N. Brothers, K. N. Kudin, V. N. Staroverov, T. A. Keith, R. Kobayashi, J. Normand, K. Raghavachari, A. P. Rendell, J. C. Burant, S. S. Iyengar, J. Tomasi, M. Cossi, J. M. Millam, M. Klene, C. Adamo, R. Cammi, J. W. Ochterski, R. L. Martin, K. Morokuma, O. Farkas, J. B. Foresman, D. J. Fox, Wallingford, CT, **2016**.

[2] X. Cai, D. Chen, K. Gao, L. Gan, Q. Yin, Z. Qiao, Z. Chen, X. Jiang, and S.-J. Su, Adv. Funct. Mater. 2018, 28, 1704927.

[3] W. Li, M. Li, W. Li, Z. Xu, L. Gan, K. Liu, N. Zheng, C. Ning, D. Chen, Y.-C. Wu, S.-J. Su, *ACS Appl. Mater. Interfaces,* **2021**, *13*(4), 5302-5311.

[4] a) Z. Shuai, *Chin. J. Chem.* **2020**, *38*, 1223-1232; b) Z. Shuai, Q. Peng, *Natl. Sci. Rev.* **2017**, *4*, 224-239; c) Z. Shuai, Q. Peng, *Phys. Rep.* **2014**, *537*, 123-156.